Electric and magnetic resonances in broadside coupled split-ring resonators: An extended mode-expansion theory

Xueqin Huang (黄学勤),[1] Yi Zhang (张忆),[1] S. T. Chui (徐少达),[2] and L. Zhou (周磊)[1,*]

[1]*Surface Physics Laboratory (State Key Laboratory) and Physics Department, Fudan University, Shanghai 200433, People's Republic of China*

[2]*Bartol Research Institute and Department of Physics and Astronomy, University of Delaware, Newark, Delaware 19716, USA*

(Received 24 January 2008; published 5 June 2008)

We extend the previously established mode-expansion theory to study the eigenmodes of metallic ring systems made by thin wires possessing filmlike rectangular cross sections. Applications of the theory to a single split-ring resonator (SRR) yield essentially the same results with finite-difference-time-domain (FDTD) simulations on realistic structures, which justify some basic assumptions adopted in the theory. We then apply the theory to study the resonance properties of a broadside coupled split-ring resonator and show that such a *planar* resonator exhibits magnetic responses along *all three* dimensions under different conditions. FDTD simulations on realistic structures are performed to successfully verify the predictions based on the extended mode-expansion theory and reveal that mutual-SRR interactions in a periodic SRR array may lead to a significant change of the eigenmode properties, including a reversal of the frequency sequence for two resonance modes. We finally employ FDTD simulations to design a realistic *layered* metamaterial that exhibits magnetic responses along all three dimensions.

DOI: 10.1103/PhysRevB.77.235105 PACS number(s): 41.20.Jb, 42.60.Da, 78.20.Bh, 78.67.−n

I. INTRODUCTION

Stimulated by recently demonstrated left-handed metamaterials (LHM) and their many fascinating electromagnetic (EM) properties,[1–3] microstructures that can provide negatively magnetic responses have attracted considerable attention. The split-ring resonator[4] (SRR) was proposed as the first candidate to realize a negative μ for **B** field along the direction normal to the ring, and then many of its topological equivalents, such as rectangular SRRs, were investigated.[3,5–11] Recently, there were much interests in new types of resonant structures such as the rod-pair structure[12,13] and the fishnet structure,[14,15] which were demonstrated to also exhibit negatively magnetic responses under certain conditions. However, all these proposed resonant structures can provide magnetic responses usually only along *one* or *two* specific directions. In order to obtain a metamaterial that has magnetic responses along all three dimensions, one needs to rotate the proposed resonant elements and combine them with the original ones to fabricate a composite material with complex microstructures. Recently, the designs and fabrications of isotropic SRRs have also drawn intensive attention.[16–23]

Extensively theoretical studies have been performed on the EM properties of the available resonance units, particularly the SRR structures. These studies include analytical ones with effective circuit parameters determined empirically[4,24,25] and brute-force numerical simulations[6–9] on realistic structures. Within the quasistatic approximation (QSA), we recently proposed an analytical theory to calculate the EM eigenmodes of a metallic ring system made by wires of *circular* cross sections,[26] and applied the theory to study a double-ring SRR in which the two rings are placed on the same plane (denoted by *coplanar* double-ring SRR in what follows).[27] The essential idea in our theory is to expand every quantity (current, inductive and/or capacitive field, resistivity, etc.) to Fourier series and then derive explicit expressions to calculate the inductance and/or capacitance parameters for *every* Fourier components in terms of the geometrical parameters. By doing so, our theory has taken account of the inductive and/or capacitive effects *completely* through considering all Fourier modes and calculated those circuit parameters *rigorously* (within the QSA). The obtained results were in excellent agreements with those obtained with brute-force numerical simulations.[26,27] However, there is an important limitation that makes our theory inapplicable to more realistic situations. While we assumed the wire forming the SRR to have a circular cross section,[26,27] this is not generally the case in practical situations, where the wire usually possesses a filmlike rectangular cross section.[2,4,28–33]

The motivations of the present work are to extend the mode-expansion theory[26,27] to more realistic situations and to search for new resonant units which have better EM properties. In this paper, based on several reasonable assumptions, we extend the mode-expansion theory to the situations where the wires forming the ring possess filmlike rectangular cross sections (denoted as *flat wires* in what follows). As a benchmark test, we first apply the theory to study a single-ring SRR made with flat wires and show that the obtained resonance frequencies are in excellent agreement with finite-difference-time-domain (FDTD) simulations on realistic structures. As another illustration, we then employ the theory to *re-examine* the broadside coupled SRR (BC-SRR) structure first proposed by Marques and coworkers[30–32] which consists of two identical split rings placed on different planes separated a small vertical distance. We show that such a resonator possesses rich electric/magnetic resonance properties. In particular, such a planar resonator with certain geometry exhibits magnetic responses along all three directions at some particular frequency. We finally perform accurate FDTD simulations on realistic structures to successfully demonstrate all theoretical predictions based on the extended

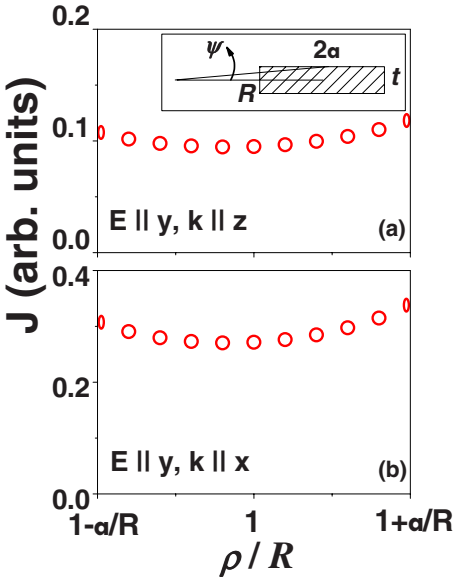

FIG. 1. (Color online) Surface current density versus ρ on the flat wire of a single-ring SRR at a fixed angle $\phi=\pi$, calculated by FDTD simulations. Here, the SRR is illuminated by plane EM waves with (a) $\vec{E}\|\hat{y}$, $\vec{k}\|\hat{z}$ and (b) $\vec{E}\|\hat{y}$, $\vec{k}\|\hat{x}$; the geometrical parameters of the single-ring SRR are $R=16$ mm, $a=1$ mm, $t=0.2$ mm and the gap width $\Delta=\pi/36$. Inset shows schematically the geometry of the rectangular cross section of the single-ring SRR.

mode-expansion theory and design a realistic structure to exhibit three-dimensional (3D) magnetic responses at the same frequency.

The present paper is organized as follows: In the Sec. II, we establish the extended mode-expansion theory for flat-wire cases with some reasonable assumptions. We then apply the theory to study a single-ring flat-wire SRR and compare the calculated results with brute-force numerical calculations in Sec. III. Section IV contains the discussions on the EM properties of a BC-SRR, with predictions fully supported by FDTD simulations on realistic systems, including both the SRR arrays and a single resonator. In Sec. V, we employ FDTD simulations to design a realistic metamaterial that possesses magnetic responses along all three dimensions at the same frequency. Finally we conclude our paper in Sec. VI.

II. MODE-EXPANSION THEORY FOR METALLIC RINGS MADE BY FLAT WIRES

We consider a single ring of a radius R placed on the x-y plane to establish our theory. The metallic ring is made from a flat wire with a rectangular cross section defined by $t \times 2a$, where $2a$ and t are the width and thickness of the wire, as schematically shown in the inset to Fig. 1(a). We focus on the situation that $R \gg 2a \gg t$, which is generally the case in practice.[2,4,28–33] Following the mode-expansion theory established in Ref. 26, we need to first understand the distribution of the current flowing in the metallic flat wire. In general, the current distributions over the rectangular cross section should be very complicated and depend on the concrete form of the probing field. For a good metal, however, the skin effect dictates that the current should mainly distribute on the metal surface, within a thin layer of a thickness equal to the metal skin depth. Since $t \ll 2a$, we can neglect the current flowing along the two side surfaces located at $r=R\pm a$ and model the true current distributions as two identical current sheets located at $z=\pm t/2$. Noting that $a \ll \lambda$ with λ being the wavelength of the probing EM wave of interest, we further take an approximation to assume that the current distributes *uniformly* along the wire width. Collecting all these considerations, we can write the current distribution as:

$$\vec{j}(\vec{r}) = \begin{cases} j(\phi)\cdot t_\delta[\delta(z+t/2)+\delta(z-t/2)]\vec{e}_\phi, & \rho \in [R-a, R+a] \\ 0, & \text{otherwise} \end{cases}, \tag{1}$$

where $t_\delta \ll t$ is the skin depth of the metal.

To verify the above assumptions, we performed FDTD simulations to study the current distributions on the flat-wire SRRs. We considered two different situations that the SRR was illuminated by a plane EM wave with $\vec{E}\|\hat{y}, \vec{k}\|\hat{z}$ or $\vec{E}\|\hat{y}, \vec{k}\|\hat{x}$, and computed the surface current distributions on the flat wires by using $\vec{J}=\vec{n}\times\vec{H}$. Here, $\vec{E}$, $\vec{H}$, and $\vec{k}$ denote the electric field, magnetic field, and the wave vector of the plane EM wave, correspondingly. The results were shown in Figs. 1(a) and 1(b), from which we found that the current distribution is indeed *nearly uniform* along the wire width, justifying Eq. (1) that we have assumed.[34–36]

With the current distributions known, we now follow the procedures of the mode-expansion theory[26] to derive the required equations for the flat-wire situations. First, consider the inductance parameters. Different from the circular cross-section case which possesses a well-defined symmetry,[26] here in the flat-wire case, the inductive field $\vec{E}_L(\rho,\phi)$ has a *nonlocal* relation with the current distribution for the coordinate ρ. Specifically, $\vec{E}_L(\rho,\phi)$ not only depends on the current density at the local point (ρ,ϕ), but also depends on the current density at a general point (ρ',ϕ'). The nonlocal problem for the coordinate ϕ is solved later by the Fourier transformation in the spirit of the mode expansion. However, the nonlocal problem for index ϕ is difficult to handle and makes it difficult to define the inductance parameters of the structure unambiguously. To solve this problem, we average both $\vec{E}_L(\vec{r})$ and $\vec{j}(\vec{r}')$ over the cross-section area of the wire in which the current flows and then set up the relationship between the two averaged quantities. By doing do, we can define the circuit parameters unambiguously and derive the explicit expressions to calculate these circuit parameters. We follow with Eq. (1) and define the averaged inductive field to be

$$\bar{E}_L(\phi) = \frac{\int \vec{E}_L(\rho,z,\phi)\cdot\vec{e}_\phi t_\delta[\delta(z+t/2)+\delta(z-t/2)]dzd\rho}{\int t_\delta[\delta(z+t/2)+\delta(z-t/2)]dzd\rho}, \tag{2}$$

After a tedious but straightforward derivation (see Appendix A), we obtain

$$E_L^m = -i\omega(L_m + L'_m)I_m/2, \tag{3}$$

where E_L^m and I_m are the Fourier components of the averaged electric field $\bar{E}_L(\phi)$ and the current $I(\phi)=j(\phi)\cdot 4at_\delta$, and L_m, L'_m are the inductance parameters. The capacitance parameters were calculated similarly,

$$E_C^m = -\frac{1}{2}\frac{1}{i\omega}\left(\frac{1}{C_m}+\frac{1}{C'_m}\right)I_m, \tag{4}$$

where E_C^m are the Fourier components of the capacitive field and C_m, C'_m are the inductance parameters. For the present flat-wire system with $t \ll R$, it is shown in Appendix A that $L'_m \approx L_m$ and $1/C'_m \approx 1/C_m$. Therefore, we can further simplify Eqs. (3) and (4) as

$$\begin{cases} E_L^m = -i\omega L_m I_m \\ E_C^m = -\dfrac{I_m}{i\omega C_m} \end{cases} \tag{5}$$

for the flat-wire case with $t/R \to 0$.

We note that Eq. (5) can also be derived assuming that the current across the flat wire takes a uniform distribution, i.e.,

$$\vec{j}(\vec{r}) = \begin{cases} j(\phi)\cdot t\cdot\delta(z)\vec{e}_\phi, & \rho\in[R-a,R+a] \\ 0, & \text{otherwise} \end{cases}. \tag{6}$$

This fact indicates that the current distribution Eq. (1) can be further simplified as Eq. (6). The physics underlying this simplification lies on the following two facts: First, when $t \ll R$, the differences between the self-interaction contributions (L'_m, C'_m, etc.) and the mutual-interaction ones (L'_m, C'_m, etc.) approach zero. Second, all those circuit parameters do not depend on the thickness of the current sheet t_δ.

With all circuit parameters known, we follow the mode-expansion theory established in Ref. 26 to set up the circuit equation,

$$\sum_{m'}\left[\tilde{\rho}(m-m') + i\left(\omega L_m - \frac{1}{\omega C_m}\right)\delta_{mm'}\right]I_{m'} = E_m^{\text{ext}}, \tag{7}$$

where $\tilde{\rho}(m)$ and E_m^{ext} are the Fourier components of the resistivity function of the ring $\tilde{\rho}(\phi)$ and the external driven field $E^{\text{ext}}(\phi)$. We then solve the matrix problem [Eq. (7)] to calculate the eigenmode properties of the flat-wire SRR, including the resonance frequency, the dipole moments under arbitrary external probing fields, etc.

III. APPLICATIONS TO A SINGLE-RING FLAT-WIRE SPLIT-RING RESONATOR

In order to justify the approximations that we adopted, we apply the theory to study the eigenmode properties of a single-ring SRR made with flat wires and compare our results with brute-force FDTD simulations on realistic systems. For a single-ring SRR with geometrical parameters set as $a/R=0.05$, gapwidth $\Delta=\pi/36$, we solved the circuit Eq. (7) with the current distribution given by Eq. (6). Numerical calculations show that the lowest resonance frequency is $\omega_1=0.457\omega_0$, independent of the film thickness t, which is shown by a dashed line in Fig. 2. Here, $\omega_0=c/R$ is the frequency unit of the present problem with c as the speed of light. If we adopt the more realistic current distribution form Eq. (1), we found that the resulting resonance frequency exhibits a very weak dependence on the parameter t, also shown in Fig. 2 by the solid line. We performed FDTD simulations on a series of realistic single-ring SRRs with $R=10$ mm, $2a=1$ mm, $\Delta=\pi/36$, and different values of t. The lowest resonance frequencies of these SRRs obtained by FDTD simulations are shown as solid stars in Fig. 2, which are in good agreements with the numerical results obtained from the extended mode-expansion theory. Such a good agreement justifies the basic assumptions [i.e., the current distribution Eq. (6)] that we adopted to derive the extended mode-expansion theory. In particular, the FDTD simulations confirmed that the resonance frequency is indeed almost *independent* of the film thickness for the flat-wire SRR, which is consistent with our arguments leading to the simplified current distribution Eq. (6).

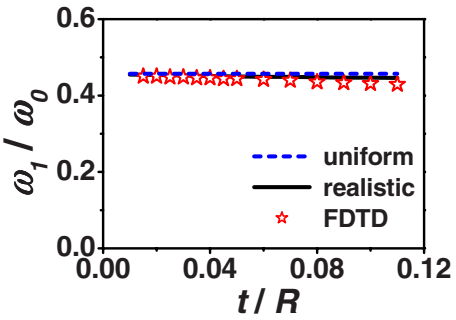

FIG. 2. (Color online) Lowest resonance frequencies of a single-ring flat-wire SRR obtained by the extended mode-expansion theory with current distribution form assumed as a uniform one Eq. (6) (dashed line) and as more realistic form Eq. (1) (solid line), and by FDTD simulations (solid stars) as functions of the thickness t, with $R=10$ mm, $2a=1$ mm, and $\Delta=\pi/36$.

IV. EIGENMODE PROPERTIES OF THE BROADSIDE COUPLED SPLIT-RING RESONATOR

Encouraged by the good results obtained for a single-ring SRR, we now apply the theory to study another type of resonator – a BC-SRR consisting of two identical split rings placed on different planes, with one ring having a small gap at $\phi=0$ while another ring having a small gap at $\phi=\pi$. In Ref. 27, we studied the resonance properties of a coplanar double-ring SRR with the wire of a circular cross section forming the SRR. The BC-SRR was first proposed by Marques *et al.*[30] and its properties were extensively studied by the same group in Refs. 31 and 32 using numerical simulations. Here we employed the extended mode-expansion

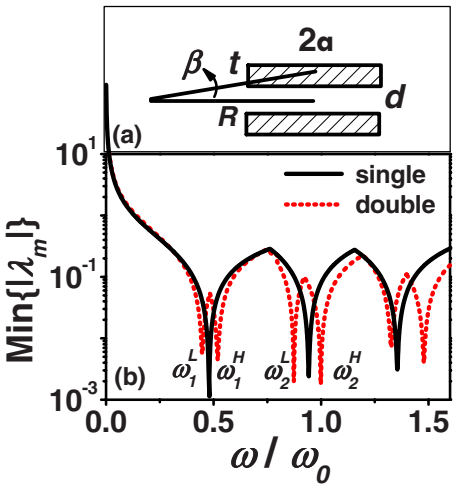

FIG. 3. (Color online) (a) Schematic figure showing the cross section of the BC-SRR. (b) Min$\{|\lambda_m|\}$ as a function of ω/ω_0 for a single-ring SRR (solid line) and a BC-SRR (dashed line). Here $R=4$ mm, $2a=0.2$ mm, $t=0.05$ mm, $d=3$ mm, and $\Delta=\pi/40$.

theory to re-examine the eigenmode properties of the BC-SRR. Our results confirmed many observations noted previously, such as the eigenmode splitting and the suppression of the bianiostropy effect.[30–32] We found several interesting physics related to such structures, which were not found in the coplanar double-ring SRRs.[27] We now describe our results in details.

A. Results of the extended mode-expansion theory

The geometry of the BC-SRR is shown schematically in Fig. 3(a). Following Refs. 26 and 27, we find that the circuit equation for the BC-SRR should be

$$\sum_{m'j'} H_{\{mj\},\{m'j'\}} I_{m'j'} = E^{\text{ext}}_{mj}, \tag{8}$$

where the matrix elements are

$$H_{\{mj\}.\{m'j'\}} = \rho_j (m-m')\delta_{jj'} + i\left(\omega L_m^{jj'} - \frac{1}{\omega C_m^{jj'}}\right)\delta_{mm'}. \tag{9}$$

Here, $j,j'=1,2$ label the two rings, m,m' denote the Fourier components, $L_m^{11}=L_m^{22}=L_m$ and $C_m^{11}=C_m^{22}=C_m$ are the self-inductive and capacitive parameters, which have been defined in Eqs. (A8) and (A15), and $L_m^{12}=L_m^{21}=\tilde{L}_m$ and $C_m^{12}=C_m^{21}=\hat{C}_m$ are the mutual inductance and/or capacitance parameters, whose forms can be found in Appendix A.

Now, diagonalize the matrix $\mathbf{H}$ as defined in Eq. (8) with a transformation matrix $\mathbf{Q}$, $\mathbf{Q}^{-1}\mathbf{H}\mathbf{Q}=\text{diag}[\lambda_1,\lambda_2,\lambda_3,\ldots]$, we find that the matrix Eq. (8) becomes $\tilde{I}_k=\tilde{E}_k^{\text{ext}}/\lambda_k$, where $\tilde{I}_k=\sum_{m'j'}(Q^{-1})_{k,\{m'j'\}}I_{\{m'j'\}}$ and $\tilde{E}_k^{\text{ext}}=\sum_{m'j'}(Q^{-1})_{k,\{m'j'\}}E^{\text{ext}}_{\{m'j'\}}$. The resonance frequencies can be determined by the condition of Min$\{|\lambda_k|\}=0$.[26] Following Refs. 26 and 27, we could compute all nonzero dipole moments of the present system induced by the external driven field. Specifically, according to the formula $\vec{m}=1/2\int(\vec{r}\times\vec{j})d\vec{r}$, we find that all three components of the magnetic-dipole moments are nonzero and given by

$$\begin{cases} m_x = -\dfrac{\pi dR}{4}\displaystyle\sum_k \frac{\tilde{E}_k^{ext}}{\lambda_k}(Q_{\{-11\},k}+Q_{\{11\},k}-Q_{\{-12\},k}-Q_{\{12\},k}) \\ m_y = -\dfrac{\pi dR}{4i}\displaystyle\sum_k \frac{\tilde{E}_k^{ext}}{\lambda_k}(Q_{\{-11\},k}-Q_{\{11\},k}-Q_{\{-12\},k}+Q_{\{12\},k}) \\ m_z = \pi R^2 \cdot \displaystyle\sum_k \frac{\tilde{E}_k^{ext}}{\lambda_k}(Q_{\{01\},k}+Q_{\{02\},k}) \end{cases} \tag{10}$$

Similarly, according to the formula $\vec{p}=\int\vec{r}\rho_e(\vec{r})d\vec{r}$, where ρ_e is the charge density, we find that the nonzero components of electric-dipole moments are

$$\begin{cases} p_x = \dfrac{\pi R}{\omega}\cdot\displaystyle\sum_k \frac{\tilde{E}_k^{\text{ext}}}{\lambda_k}(Q_{\{-11\},k}-Q_{\{11\},k}+Q_{\{-12\},k}-Q_{\{12\},k}) \\ p_y = \dfrac{\pi R}{i\omega}\cdot\displaystyle\sum_k \frac{\tilde{E}_k^{\text{ext}}}{\lambda_k}(Q_{\{-11\},k}+Q_{\{11\},k}+Q_{\{-12\},k}+Q_{\{12\},k}) \end{cases}. \tag{11}$$

Several interesting features are noted from analyzing Eqs. (10) and (11). First, we find that the present system can offer magnetic polarization along *all* three dimensions under different conditions, in sharp contrast to other resonating units which typically can only provide magnetic response along certain directions.[3] Second, while the m_z component is (roughly) proportional to the area of the ring $\sim\pi R^2$, we find that the two transverse magnetizations, m_x,m_y, are (roughly) proportional to the cross-section area sandwiched between the two rings $\sim d\cdot R$ [see Eq. (18)]. Therefore, an intuitive expectation is that the transverse dipole moments can be enhanced through enlarging the inter-ring separation d. Finally, we find from comparing Eq. (10) with Eq. (11) that the m_x polarization is closely related to the p_y polarization [both proportional to $(Q_{\{-1j\},k}+Q_{\{1j\},k})$ for the j^{th} ring] and the m_y polarization is closely related to the p_x polarization [both proportional to $(Q_{\{-1j\},k}-Q_{\{1j\},k})$ for the j^{th} ring]. More interestingly, we find that the way that the two rings contribute to the electric polarization is just *opposite* to that the two rings contribute to the magnetic polarization. Let us check the dipole moments m_x,p_y as an example. Suppose the currents flowing on the two rings are in-phase so that the $Q_{\{mj\},k}$ elements are of the same sign for the two rings, we find that the contribution to p_y from the two rings are *constructively* adding to each other and the contribution to m_x from the two rings are *destructively* canceling each other. Similar arguments hold for the two dipole moments m_y,p_x. In fact, these peculiar eigenvector properties directly lead to the complete suppressions of the bianisotropy of all eigenmodes in present systems, which we will discuss later.

We now quantitatively study a model system with parameters set as $R=4$ mm, $2a=0.2$ mm, $t=0.05$ mm, and $d=3$ mm. A gap of a width $\Delta=\pi/40$ is opened at $\phi=0$ for the upper ring and at $\phi=\pi$ for the lower ring. The amplitude of

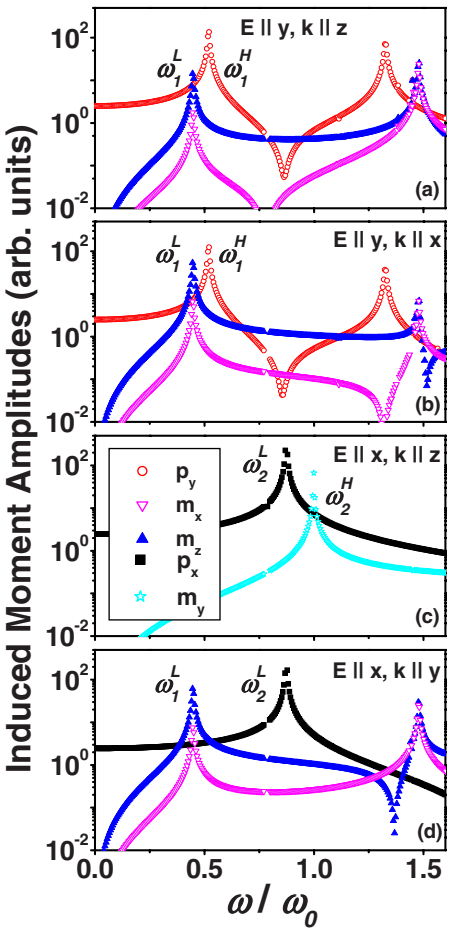

FIG. 4. (Color online) Amplitudes of the induced moments of the BC-SRR as functions of ω/ω_0, calculated by the extended mode-expansion theory with different types of plane waves with E field and wave propagation directions as shown in the figure.

the lowest eigenvalue is shown in Fig. 3(b) as a function of the reduced frequency; that of a single-ring SRR of the same size is also shown in the figure as a reference. We note that the size of this particle (~8 mm) is much smaller than wavelength at resonance (~55 mm for the first mode), and thus it can serve as a building block in metamaterials. Compared with the spectrum of the single-ring SRR, we find that each single-ring mode has split into a pair of two modes with different symmetries, caused by the mutual-ring interactions. We follow the labeling scheme adopted in Ref. 27 to denote the lower and higher modes split from the k^{th} single-ring mode (ω_k) as ω_k^L, ω_k^H, respectively. Such a mode splitting behavior is quite similar to the coplanar double-ring SRR case[27] and has also been noted previously.[32] However, when we studied the dipole moments related to these resonance eigenmodes, we find the present system exhibits *richer* EM properties than a coplanar double-ring SRR.[27] In particular, in addition to the perpendicular magnetic polarization m_z, two more in-plane polarization m_x, m_y can also be induced for the BC-SRR under specific conditions.

We have calculated the dipole moments of the present structure induced by four different types of external field excitations and shown these moments in Figs. 4(a)–4(d). From the figures we can clearly identify the dipole moments related to each eigenmode of the double-ring system; thus, the peaks of the moments are labeled by the corresponding eigenfrequencies. We summarize the characteristics of the EM polarizations for the lowest four modes in Table I. All these modes are *completely free of bianisotropy* (i.e., either purely magnetic or purely electric). This important character has also been noted previously in Refs. 30–32.

Let us first consider the mode pair (ω_1^L, ω_1^H) which originate from the first single-ring mode ω_1. From our previous work,[26] we understand that the ω_1 mode carries both electric and magnetic polarizations (p_y, m_z), which have also been recorded in Table I. For the BC-SRR, the ω_1^L mode only carries the m_z moment and the ω_1^H mode only carries the p_y moment, due to the symmetry of each mode. The most interesting character is that a *new* dipole moment m_x appears for the ω_1^L mode, which does not exist for the corresponding single-ring mode[26] and the coplanar double-ring SRR.[27] This is also consistent with our previous observation that the m_x moment is closely related to the p_y polarization in the present BC-SRR [see discussions following Eqs. (10) and (11)].

We next consider the mode pair ω_2^L, ω_2^H. Since our previous study reveals that the single-ring ω_2 mode exhibits only the p_x polarization,[26] it is not surprising to see that the mode ω_2^L still carries the p_x polarization, as recorded in Table I. Equivalently speaking, the ω_2^L mode is now an *electric* mode. However, for the ω_2^H mode, the p_x polarization *disappears* and a new polarization m_y is induced, implying that the ω_2^H mode is a pure *magnetic* mode. The appearance of this polarization is quite unexpected, since both a single-ring SRR (Ref. 26) and a coplanar double-ring SRR (Ref. 27) do not carry the m_y polarization, and in fact, the corresponding single-ring mode is a purely electric mode without magnetic moments at all.[26]

TABLE I. Characteristics of electric/magnetic polarizations of low-lying modes for a BC-SRR and a single-ring SRR.

System	Mode	p_x	p_y	m_z	m_x	m_y
Single	ω_1	No	Yes	Yes	No	No
Double	ω_1^L	No	Disappear	Enhanced	New	No
	ω_1^H	No	Enhanced	Disappear	No	No
Single	ω_2	Yes	No	No	No	No
Double	ω_2^L	Enhanced	No	No	No	No
	ω_2^H	Disappear	No	No	No	New

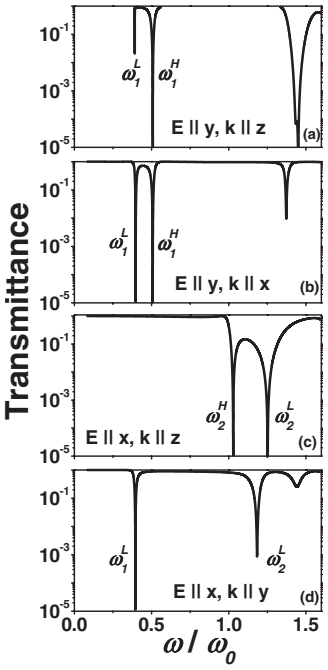

FIG. 5. FDTD-calculated transmission spectra with the same probing EM waves as in Fig. 4.

B. Finite-difference-time-domain results on split-ring resonator arrays

We now perform FDTD simulations on realistic ring structures to verify the theoretical predictions recorded in Table I. The geometrical parameters of the BC-SRR that we adopted in FDTD simulations are that $R=4$ mm, $2a=0.2$ mm, $t=0.05$ mm, and $d=3$ mm. A gap of a width $\Delta=\pi/40$ is opened at $\phi=0$ for the upper ring and at $\phi=\pi$ for the lower ring. To probe the eigenresonances of the structure, we follow the calculation scheme as described in Refs. 26 and 27 to compute the EM wave transmissions through slabs consisting of periodic arrays of such BC-SRRs. We adopted four types of input EM waves with exactly the same configurations as specified in Figs. 4(a)–4(d) to illuminate these slabs and depicted the transmission spectra in Fig. 5(a)–5(d), correspondingly. For configurations (a) and (c), the slab is constructed by repeating the unit resonance structure with lattice constants $b=16$ mm in the x-y plane. Similarly, we repeat the unit cell with lattice constants $b=16$ mm in the y-z or x-z plane to form a slab for configuration (b) or (d). Comparing the transmission spectra shown in Fig. 5 with the dipole moment spectra depicted in Fig. 4, we find a one-by-one correspondence between the transmission dips and the moment peaks. We then label the modes in Fig. 5 identified through comparing with Fig. 4.

For the first mode pair (ω_1^L and ω_1^H), we find that the FDTD transmission spectra agree quite well with the moment spectra calculated under different configurations. For example, theoretical analyses indicate that the first mode ω_1^L carries two magnetic-dipole moments m_z and m_x, and therefore, EM waves with configurations (a), (b), and (d) can excite such a resonance since **B** fields are along x, z, and z directions in these cases. Indeed, FDTD transmission spectra depicted in Figs. 5(a), 5(b), and 5(d) show clearly that there is a dip at the same frequency $\omega=0.394\omega_0$, which is easily identified as ω_1^L. Similar arguments hold for the second mode ω_1^H.

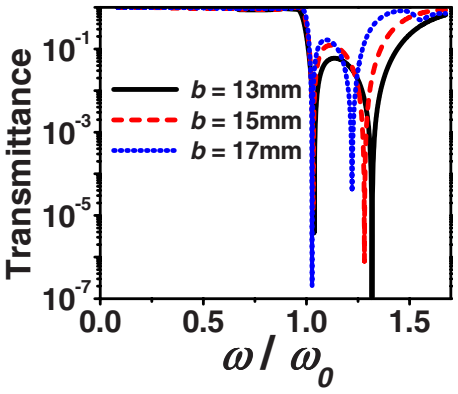

FIG. 6. (Color online) FDTD-calculated transmission spectra through SRR arrays with different lattice constants b, with the input EM wave taking $\vec{E}\|\hat{x}$, $\vec{k}\|\hat{z}$.

Things are quite different for the second mode pair (ω_2^L and ω_2^H). Theoretical analysis based on the mode-expansion theory suggests that the lower-frequency mode ω_2^L should be an electric mode carrying an enhanced p_x polarization and the higher-frequency mode ω_2^H a magnetic mode carrying m_y polarization (see Table I). Therefore, EM waves with configurations (c) and (d) should excite the electric mode since the **E** fields are along the x direction in these two cases; but only the EM wave with configuration (c) can excite the magnetic mode because of $\vec{B}\|\hat{y}$. Such resonance properties are also consistent with the dipole moment spectra depicted in Figs. 4(c) and 4(d). However, when we compare the FDTD transmission spectra [Figs. 5(c) and 5(d)] with the corresponding dipole moment spectra [Figs. 4(c) and 4(d)], we find that the lower-frequency mode should be identified as a magnetic mode, but the higher-frequency mode should be identified as an electric mode, as already labeled in the spectra. Clearly, this is *inconsistent* with our theoretical analysis, but the question is: *what causes such a contradiction.*

We find such discrepancies are induced by the mutual interactions between different resonance units in the slab models adopted in our FDTD simulations, whereas, the theoretical analysis in Sec. IVA is based on a single BC-SRR. To understand the role of mutual interactions, we varied the lattice constant b of the SRR array and then calculated the transmission spectra through such SRR arrays, with the input wave configuration fixed as $\vec{E}\|\hat{x},\vec{k}\|\hat{z}$ [i.e., those of Fig. 4(c) and Fig. 5(c)]. The FDTD calculated transmission spectra for SRR arrays with different periodicities were compared in Fig. 6. Comparison between different spectra shows that the transmission dips, and in turn, the resonance mode positions, do strongly depend on the lattice constant (and in turn, the mutual-SRR interactions). We show in Fig. 7 the two resonance frequencies as functions of the lattice constant, with the resonance frequencies of a single resonator calculated by the mode-expansion theory depicted as dotted and dashed lines as references. When the lattice constant increases lead-

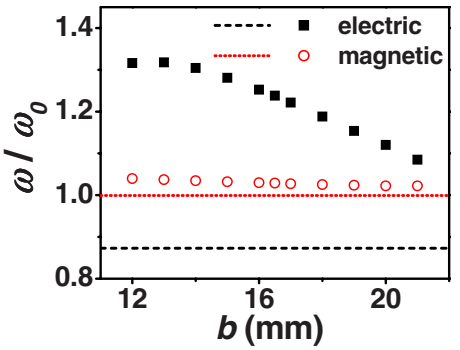

FIG. 7. (Color online) FDTD-calculated frequencies of the ω_2^L mode (electric, solid squares) and the ω_2^H mode (magnetic, open circles) as functions of the lattice constant of the SRR arrays. The dotted and the dashed lines are the theoretical values of the ω_2^H mode and the ω_2^L mode, calculated by the mode-expansion theory for a single resonator.

ing to a weakened mutual-resonator interaction, the electric (ω_2^L) mode shifts downward significantly while the magnetic (ω_2^H) mode remains almost unchanged. There is a critical value of lattice constant at which the two modes merge together. However, when the lattice constant increases further, we find it difficult to clearly identify the electric mode since its strength is too weak. Nevertheless, these facts indicate that the mutual SRR interactions must be responsible for the reversal of the two resonance modes.

C. Finite-difference-time-domain results on a single broadside coupled split-ring resonator

To further clarify the role of the mutual-SRR interactions, we employ the FDTD simulations to *directly* study the responses of a single resonant unit. Under monochromic external plane waves with different frequencies and polarizations, we calculated the electric currents induced at a particular point on the surface of the top ring of the SRR using the formula $\vec{J}=\vec{n}\times\vec{H}$ and identified the resonance modes of the BC-SRR by the condition that J reaches a maximum. The calculated results were shown in Fig. 8(b). Compared with the spectrum of $\mathrm{M}in|\lambda_m|$ calculated by the mode-expansion theory and reproduced in Fig. 8(a), we can clearly identify three modes, ω_1^L, ω_1^H, and ω_2^H, whose positions are in excellent agreements with the theoretical values. However, the mode ω_2^L is too weak to be detectable from Fig. 8(b). This is also consistent with the FDTD simulations on SRR arrays with very large lattice constants, as explained in Sec. IVB. The physics is that the nearby magnetic mode ω_2^H is too strong; the tail of this mode extends to the regime of the electric mode ω_2^L and overwhelms it. To search for the missing electric mode ω_2^L, we further calculated a new quantity $\vec{J}_T=\vec{J}_1+\vec{J}_2$, which is a sum of the currents induced on the two rings (at the same ϕ position). Clearly, the total current $\vec{J}_T$ should exhibit a maximum at an electric resonance but not at a magnetic resonance, so that examining this quantity helps us isolate the missing electric mode from the strong background of the magnetic resonance. Indeed, as shown in Fig.

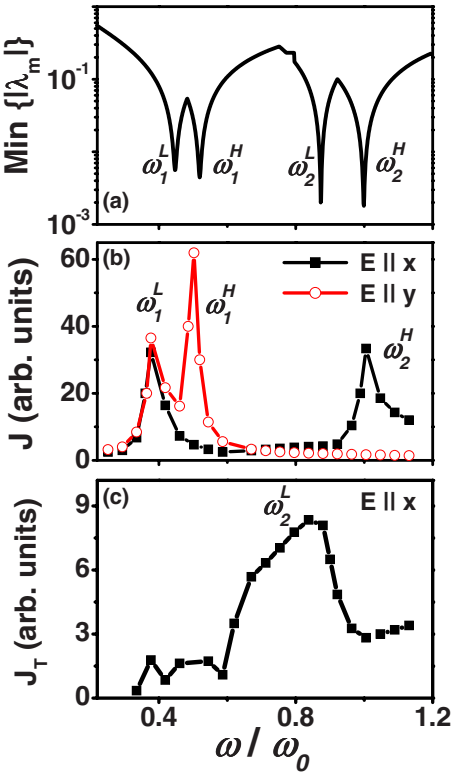

FIG. 8. (Color online) (a) $\mathrm{M}in|\lambda_m|$ as a function of ω/ω_0 for the BC-SRR with geometrical parameters same as that studied in Fig. 3. (b) Amplitudes of the maximum surface current density measured on the top ring of the BC-SRR as functions of frequency, with input plane waves taking $\vec{E}\|\hat{x}$, $\vec{k}=(0,1/2,\sqrt{3}/2)\omega/c$ (solid squares) and with $\vec{E}\|\hat{y}$, $\vec{k}=(1/2,0,\sqrt{3}/2)\omega/c$ (open circles); (c) Amplitudes of the maximum total current density (sum of the currents flowing on the two rings at the same ϕ position) of the BC-SRR as a function of frequency, with the probing EM wave taking $\vec{E}\|\hat{x}$, $\vec{k}=(0,1/2,\sqrt{3}/2)\omega/c$.

8(c), we find that the amplitude of the total current J_T does exhibit a peak around the frequency of $0.9\omega_0$, whose position agree *excellently* with the theoretical value as compared with Fig. 8(a).

Now that we have identified the frequencies of all the resonance modes; we computed the current distributions inside the systems at these frequencies. To visualize the four modes clearly, we depicted the instantaneous magnetic-field distributions along the line normal to the ring plane in Figs. 9(a)–9(d) for the four modes. It is quite easy to identify that the first and the fourth modes are magnetic ones since there are strong magnetic field localized inside the structure. On the other hand, the second and the third modes are electric ones. These features are consistent with the theoretical analysis as recorded in Table I and resolved the puzzle of the mode sequence reversal that we found in FDTD calculations for SRR arrays (see Sec. IVB). This fact confirmed our arguments that the mutual SRR interactions do play crucial roles to lead to a reordering of the sequence of two resonance modes. To gain a more comprehensive understanding of the EM characteristics of these modes, we also showed in Figs. 9(e)–9(h) the in-plane current distributions on the upper ring

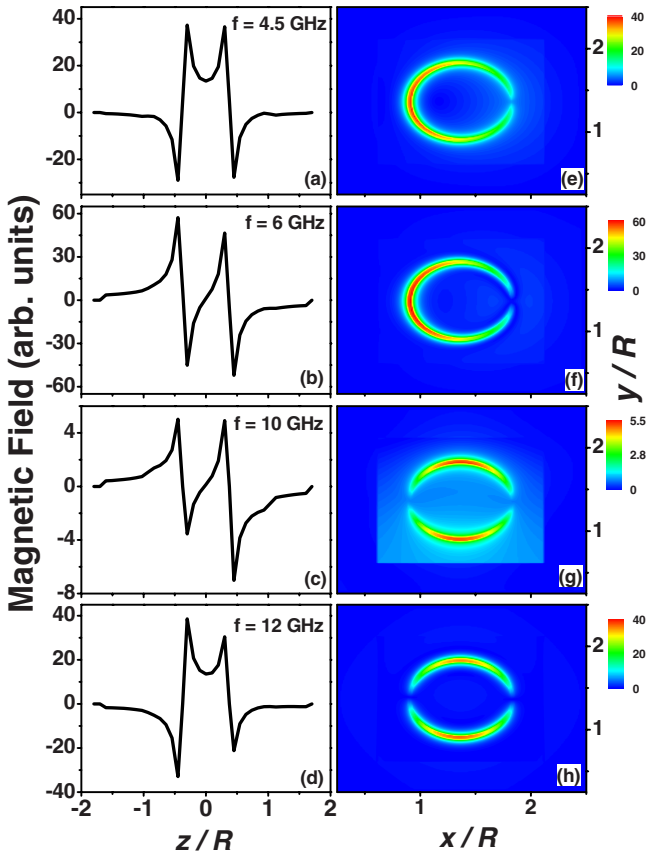

FIG. 9. (Color online) (a)–(d) FDTD-calculated instantaneous magnetic-field distributions along the line normal to the ring plane for the four resonance modes. (e)–(h) FDTD-calculated current distributions on the top ring (with a small gap opened at $\phi=0$) of the BC-SRR at the four resonance frequencies. Here, the geometrical parameters of the BC-SRR are $R=4$ mm, $2a=0.2$ mm, $t=0.05$ mm, and $d=3$ mm, and the SRR is illuminated by plane EM waves with $\vec{E}\|\hat{y}$, $\vec{k}=(1/2,0,\sqrt{3}/2)\omega/c$ for (a), (b), (e), and (f) and $\hat{E}\|\hat{x}$, $\vec{k}=(0,1/2,\sqrt{3}/2)\omega/c$ for (c), (d), (g), and (h).

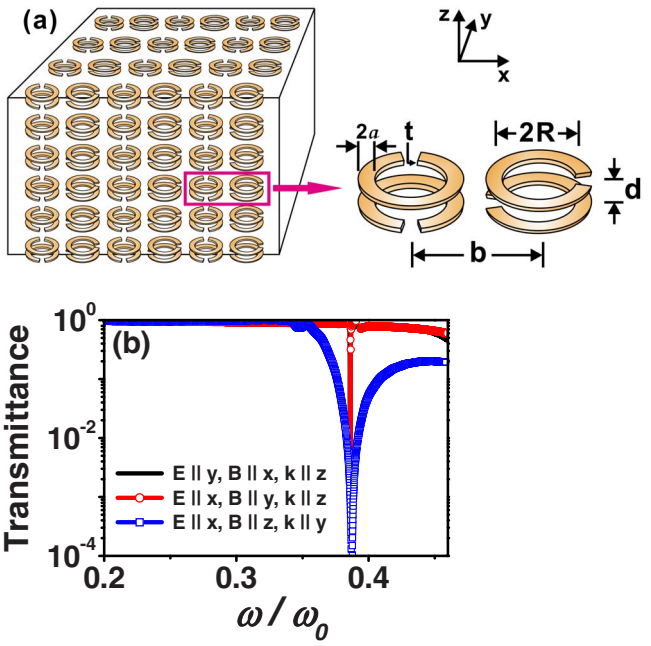

FIG. 10. (Color online) (a) A schematic picture of the designed 3D magnetic material, with the inset showing the unit cell of structure. Here, $R=4$ mm, $2a=0.2$ mm, $t=0.05$ mm, $d=3$ mm, and $b=11$ mm and the gap width $\Delta=\pi/40$. (b) FDTD-calculated transmission spectra through the designed 3D magnetic material with different probing EM waves as specified in the figure.

of the BC-SRR at those four resonance frequencies. The in-plane current distributions of the present resonator are basically the same as those of the single-ring SRR mode.[26] For example, for the third and fourth mode, the current distributions are intrinsically the same, both resembling the pattern for the ω_2 mode of the singe-ring SRR.[26] With the knowledge of the entire current distributions for every mode, we achieve a complete picture to understand the EM characteristics of all these resonance modes, which will be helpful for further applications of such resonance units in more complicated situations.

V. METAMATERIALS WITH THREE-DIMENSIONAL MAGNETIC RESPONSES

Metamaterials that possess magnetic responses along all three dimensions drew much attention recently.[16–23] As many resonant structures are inherently anisotropic, a standard method to design 3D magnetic materials is to rotate the unit-cell element and combine it with the original one to form an isotropic unit cell.[16–23] Here, we provide an alternative approach. We demonstrate that a *layered* structure, composed by planar arrays of BC-SRRs, can exhibit magnetic responses along all three dimensions at the same frequency. Since the structure is basically a multilayer system, it is very easy to fabricate, particularly in higher frequency regime where the complex 3D structures are relatively difficult to fabricate. As shown in Fig. 10, the unit cell of the designed metamaterial contains two BC-SRRs, with one rotated by 90° with respect to the other one. To understand the resonance properties of the designed system, we employed FDTD simulations to calculate the transmissions of EM plane waves with magnetic fields polarized along different directions and with different propagation directions. The transmission spectra in different cases are compared in Fig. 10(b). It is clearly shown that for **B** field along all three directions, a *common* resonance is excited at the frequency $\omega\sim 0.386\omega_0$, implying that the system exhibits strong responses to external magnetic fields along all three directions at this frequency. To identify the nature of such a resonance, we depicted the instantaneous magnetic-field distributions along the line normal to the ring plane in Fig. 11(a). The fact that strong magnetic fields are localized inside the structure is the direct signature of a magnetic resonance. We also calculated the electric currents flowing on the upper ring of the unit cell and illustrated the current distributions in Figs. 11(b) and 11(c) for two different probing EM waves specified in the figure. Clearly, the EM wave with $\vec{E}\|\hat{y}$, $\vec{B}\|\hat{x}$, and $\vec{k}\|\hat{z}$ induces m_x and m_z moments of BC-SRR on the right-hand side in the unit cell, while the EM wave with $\vec{E}\|\hat{x}$, $\vec{B}\|\hat{y}$,

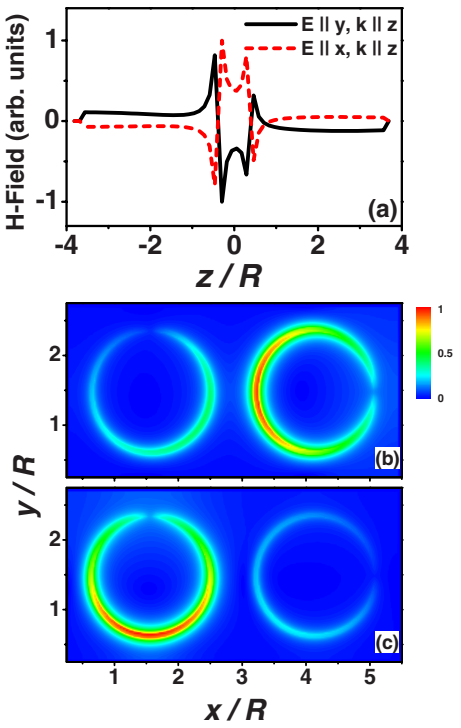

FIG. 11. (Color online) (a) FDTD-calculated instantaneous magnetic-field distributions along the line normal to the ring plane at the resonance frequency, with two different probing EM waves as specified in the figure. FDTD-calculated current distributions on the top ring of the unit cell of designed 3D material at the resonance frequency, excited by a probing EM wave with (b) $\vec{E}\|\hat{y}$, $\vec{B}\|\hat{x}$, and $\vec{k}\|\hat{z}$ and a probing EM wave (c) with $\vec{E}\|\hat{x}$, $\vec{B}\|\hat{y}$, and $\vec{k}\|\hat{z}$.

and $\vec{k}\|\hat{z}$ induces m_y and m_z moments of BC-SRR on the left-hand side, and therefore, the structure as a whole exhibits magnetic responses for all three directions at the same frequency.

VI. CONCLUSIONS

To summarize, we have successfully extended the previously established mode-expansion theory to the situations where the wire forming the ring possesses a flat rectangular cross section. Applications of the theory to a single-ring flat-wire SRR shows that the obtained results are in good agreements with brute-force FDTD simulations on realistic systems, which justified some basic assumptions adopted in deriving the theory. We then employed the theory to study the EM characteristics of a BC-SRR with two split rings placed on different planes separated by a small vertical distance and showed that such a resonator could provide magnetic responses along all three directions under different conditions. We performed brute-force FDTD simulations on realistic metallic ring structures, including both the SRR arrays and a single resonator, to successfully verify all predictions based on the theory. The FDTD results revealed that the mutual SRR interactions in a periodic SRR array may change significantly the resonance properties of the SRR, by even leading to a reordering of the mode sequence. Finally, we employ FDTD simulations to successfully design a realistic layered metamaterial that exhibits magnetic responses along all three directions at the same frequency.

ACKNOWLEDGMENTS

We thank C. T. Chan for many stimulating discussions. This work was supported by the China-973 Program (Grants No. 2004CB719800 and No. 2006CB921701), the NSFC (Grants No. 10504003 and No. 60725417), Fok Ying Tung Education Foundation, PCSIRT, and MOE of China (Grant No. B06011). S.T.C. is supported in part by the U.S. DOE.

APPENDIX A: DERIVATIONS OF CIRCUIT PARAMETERS

We consider first the inductive effects for a flat-wire single-ring SRR. Following Ref. 18, the inductive field within the QSA is found as

$$\vec{E}_L(\vec{r}) = -i\omega\frac{\mu_0}{4\pi}\int \sum_{l=0}^{\infty}\sum_{m=-l}^{l}\frac{4\pi}{2l+1}Y_{lm}(\theta,\phi)Y_{lm}^*(\theta',\phi') \times \frac{r_<^l}{r_>^{l+1}}\vec{j}(\vec{r}')d\vec{r}'. \tag{A1}$$

Putting Eq. (A1) into Eq. (2), we find that the averaged field contains two terms,

$$\bar{E}_L(\phi) = E_{Ls}(\phi) + E_{Lm}(\phi) \tag{A2}$$

where $E_{Ls}(\phi)$ is concerned with the self-inductive effect within each single surface while $E_{Lm}(\phi)$ is concerned with the mutual inductive effect between the currents flowing on the two surfaces.

Consider first the term $E_{Ls}(\phi)$. Straightforward calculations show that

$$E_{Ls}(\phi) = -i\omega\frac{\mu_0}{32\pi a^2}\sum_{m=-\infty}^{\infty}\sum_{l=|m|}^{\infty}\frac{(l-m)!}{(l+m)!}|P_l^m(0)|^2 e^{im\phi} \times \int e^{-im\phi'}\cos(\phi-\phi')I(\phi')d\phi' \times \int_{R-a}^{R+a}d\rho\int_{R-a}^{R+a}\frac{\rho_<^l}{\rho_>^{l+1}}\rho' d\rho', \tag{A3}$$

where $I(\phi)=\int\vec{j}(\vec{r})d\vec{S}=j(\phi)\cdot 4at_\delta$ is the total current flowing across the flat wire at a position defined by the angle ϕ, $P_l^m(x)$ is the usual associated Legendre function, and $\rho_>(\rho_<)$ takes the larger (smaller) value of ρ,ρ'. Expand the current as a Fourier series, $I(\phi')=\Sigma_{m'}I_{m'}e^{im'\phi'}$ and note that $\int e^{im'\phi'}e^{-im\phi'}\cos(\phi-\phi')d\phi' = \pi[e^{i\phi}\delta(m-m'+1)+e^{-i\phi}\delta(m-m'-1)]$, we can carry out the integration and get

$$E_{Ls}(\phi) = -\frac{i\omega\mu_0}{8}\sum_m A_m e^{im\phi}[I_{m+1}e^{i\phi}+I_{m-1}e^{-i\phi}] = -\frac{i\omega\mu_0}{8}\sum_m e^{im\phi}[A_{m-1}+A_{m+1}]I_m, \tag{A4}$$

where

$$A_m = \sum_{l=|m}^{\infty} \frac{(l-m)!}{(l+m)!} |P_l^m(0)|^2 \alpha_l, \tag{A5}$$

with

$$\alpha_l = \frac{1}{4a^2} \int \int_{R-a}^{R+a} \rho' d\rho \frac{\rho_<^l}{\rho_>^{l+1}} d\rho'. \tag{A6}$$

Expand $E_{Ls}(\phi)$ as a Fourier series $E_{Ls}(\phi) = \sum_{m=-\infty}^{+\infty} E_{Ls}^m \exp(im\phi)$, we find that

$$E_{Ls}^m = -i\omega L_m I_m/2, \tag{A7}$$

where

$$L_m = \frac{\mu_0}{4}[A_{m-1} + A_{m+1}] \tag{A8}$$

is *part* of the inductive parameter for the m^{th} Fourier component. The inductive parameter defined in Eq. (A8) takes *exactly* the same form as that for the circular cross-section case,[18] except the dimensionless parameter α_l is given by Eq. (A6) and is no longer of the form of $(1-a/R)^l$ in the circular cross-section case.[18]

We next consider the term $E_{Lm}(\phi)$. Again, expand $E_{Lm}(\phi)$ as a Fourier series $E_{Lm}(\phi) = \sum_{m=-\infty}^{+\infty} E_{Lm}^m \exp(im\phi)$; we find after some straightforward calculations that

$$E_{Lm}^m = -i\omega L_m' I_m/2, \tag{A9}$$

where

$$L_m' = \frac{\mu_0}{4}[A_{m-1}' + A_{m+1}'], \tag{A10}$$

with

$$A_m' = \frac{1}{4a^2} \sum_{l=|m}^{\infty} \frac{(l-m)!}{(l+m)!} |P_l^m(\sin\psi) P_l^m(- \sin\psi)| \int \int_{R-a}^{R+a} \rho' d\rho \frac{r_<^l}{r_>^{l+1}} d\rho'. \tag{A11}$$

Here, $r = \sqrt{\rho^2 + t^2/4}$, $r' = \sqrt{\rho'^2 + t^2/4}$, $\psi = \tan^{-1}(t/2R) \ll 1$ [see Fig. 1(a)], and $r_>(r_<)$ takes the larger (smaller) value of r, r'. Collecting Eqs. (A2), (A7), and (A9), we finally arrive at

$$E_L^m = -i\omega(L_m + L_m')I_m/2. \tag{A12}$$

We then consider the capacitance parameters for a flat-wire single-ring SRR. According to Ref. 18, we find the capacitive field to be

$$\vec{E}_C(\vec{r}) = \vec{e}_\phi \frac{1}{i\omega} \frac{1}{4\pi\varepsilon_0} \frac{\partial}{\rho \partial \phi} \int \sum_{l=0}^{\infty} \sum_{m=-l}^{l} \frac{4\pi}{2l+1} Y_{lm}(\theta,\phi) Y_{lm}^*(\theta',\phi') \times \frac{r_<^l}{r_>^{l+1}} \nabla' \cdot \vec{j}(\vec{r}') d\vec{r}. \tag{A13}$$

Following exactly the same procedures as in the inductance case, we derived the relationship between the averaged capacitive field $\bar{E}_C(\phi)$ and the total current $I(\phi)$. In Fourier component form, the relationship is

$$E_C^m = -\frac{1}{2} \frac{1}{i\omega} \left(\frac{1}{C_m} + \frac{1}{C_m'} \right) I_m, \tag{A14}$$

where

$$\frac{1}{C_m} = \frac{m^2}{8\varepsilon_0 a^2} \sum_{l=|m|}^{\infty} \frac{(l-m)!}{(l+m)!} |P_l^m(0)|^2 \int_{R-a}^{R+a} \frac{d\rho}{\rho} \int_{R-a}^{R+a} \frac{\rho_<^l}{\rho_>^{l+1}} d\rho' \tag{A15}$$

describes the self-capacitance effects within each single current sheet and

$$\frac{1}{C_m'} = \frac{m^2}{8\varepsilon_0 a^2} \sum_{l=|m|}^{\infty} \frac{(l-m)!}{(l+m)!} |P_l^m(\sin\psi) P_l^m(- \sin\psi)| \int_{R-a}^{R+a} \frac{d\rho}{\rho} \int_{R-a}^{R+a} \frac{r_<^l}{r_>^{l+1}} d\rho' \tag{A16}$$

describes the mutual capacitance effects between two current sheets. In the limit of $t/R \to 0$, we find easily that $\sin\psi \approx 0$, $r \approx \rho$, and $r' \approx \rho'$. Comparing Eq. (A15) with Eq. (A16) shows that $1/C_m' \approx 1/C_m$ as $t/R \to 0$. Similarly, we find $L_m' \approx L_m$ in the same limit.

We finally consider the circuit parameters for a BC-SRR. Following the same procedures presented above, we find the mutual inductance and capacitance parameters of a double ring system should be

$$\tilde{L}_m = \frac{\mu_0}{4}[\tilde{A}_{m-1} + \tilde{A}_{m+1}], \tag{A17}$$

with

$$\tilde{A}_m = \frac{1}{4a^2} \sum_{l=|m|}^{\infty} \frac{(l-m)!}{(l+m)!} |P_l^m(\sin\beta) P_l^m(-\sin\beta)| \times \int \int_{R-a}^{R+a} \rho' d\rho' \frac{r_<^l}{r_>^{l+1}} d\rho \tag{A18}$$

and

$$\frac{1}{\tilde{C}_m} = \frac{m^2}{8\varepsilon_0 a^2} \sum_{l=|m|}^{\infty} \frac{(l-m)!}{(l+m)!} |P_l^m(\sin\beta) P_l^m(-\sin\beta)| \times \int_{R-a}^{R+a} \frac{d\rho}{\rho} \int_{R-a}^{R+a} \frac{r_<^l}{r_>^{l+1}} d\rho', \tag{A19}$$

where $r = \sqrt{\rho^2 + d^2/4}$, $r' = \sqrt{\rho'^2 + d^2/4}$, and $\beta = \tan^{-1}(d/2R)$ [see the geometry shown in Fig. 3(a)].

*Corresponding author; phzhou@fudan.edu.cn

[1] V. C. Veselago, Sov. Phys. Usp. **10**, 509 (1968).
[2] D. R. Smith, W. J. Padilla, D. C. Vier, S. C. Nemat-Nasser, and S. Schultz, Phys. Rev. Lett. **84**, 4184 (2000).
[3] R. A. Shelby, D. R. Smith, and S. Schultz, Science **292**, 77 (2001).
[4] J. B. Pendry, A. J. Holden, D. J. Robbins, and W. J. Stewart, IEEE Trans. Microwave Theory Tech. **47**, 2075 (1999).
[5] J. Zhou, Th. Koschny, M. Kafesaki, E. N. Economou, J. B. Pendry, and C. M. Soukoulis, Phys. Rev. Lett. **95**, 223902 (2005).
[6] D. R. Smith, S. Schultz, P. Markos, and C. M. Soukoulis, Phys. Rev. B **65**, 195104 (2002).
[7] N. Katsarakis, T. Koschny, M. Kafesaki, E. N. Economou, and C. M. Soukoulis, Appl. Phys. Lett. **84**, 2943 (2004).
[8] P. Markos and C. M. Soukoulis, Phys. Rev. E **65**, 036622 (2002).
[9] Bogdan-Ioan Popa and S. A. Cummer, Phys. Rev. B **72**, 165102 (2005).
[10] T. J. Yen, W. J. Padilla, N. Fang, D. C. Vier, D. R. Smith, J. B. Pendry, D. N. Basov, and X. Zhang, Science **303**, 1494 (2004).
[11] S. Linden, C. Enkrich, M. Wegener, J. F. Zhou, T. Koschny, and C. M. Soukoulis, Science **306**, 1351 (2004).
[12] V. A. Podolskiy, A. K. Sarychev, and V. M. Shalaev, Opt. Express **11**, 735 (2003).
[13] G. Dolling, C. Enkrich, M. Wegener, J. F. Zhou, C. M. Soukoulis, and S. Linden, Opt. Lett. **30**, 3198 (2005).
[14] S. Zhang, W. Fan, N. C. Panoiu, K. J. Malloy, R. M. Osgood, and S. R. J. Brueck, Phys. Rev. Lett. **95**, 137404 (2005).
[15] G. Dolling, C. Enkrich, M. Wegener, C. M. Soukoulis, and S. Linden, Science **312**, 892 (2006).
[16] P. Gay-Balmaz and O. J. F. Martin, Appl. Phys. Lett. **81**, 939 (2002).
[17] C. R. Simovski and S. He, Phys. Lett. A **311**, 254 (2003).
[18] C. R. Simovski and B. Sauviac, Radio Sci. **39**, RS2014 (2004).
[19] E. Verney, B. Sauviac, and C. R. Simovski, Phys. Lett. A **331**, 244 (2004).
[20] T. Koschny, L. Zhang, and C. M. Soukoulis, Phys. Rev. B **71**, 121103(R) (2005).
[21] J. D. Baena, L. Jelinek, R. Marqués, and J. Zehentner, Appl. Phys. Lett. **88**, 134108 (2006).
[22] J. D. Baena, L. Jelinek, and R. Marqués, Phys. Rev. B **76**, 245115 (2007).
[23] J. D. Baena, L. Jelinek, and R. Marqués, Appl. Phys. Lett. **91**, 191105 (2007).
[24] M. Shamonin, E. Shamonina, V. Kalinin, and L. Solymar, J. Appl. Phys. **95**, 3778 (2004).
[25] M. Shamonin, E. Shamonina, V. Kalinin, and L. Solymar, Microwave Opt. Technol. Lett. **44**, 133 (2005).
[26] L. Zhou and S. T. Chui, Phys. Rev. B **74**, 035419 (2006).
[27] L. Zhou and S. T. Chui, Appl. Phys. Lett. **90**, 041903 (2007).
[28] B. Sauviac, C. R. Simovski, and S. A. Tretyakov, Electromagnetics **24**, 317 (2004).
[29] N. Lagarkov, V. N. Semenenko, V. A. Chistyaev, D. E. Ryabov, S. A. Tretyakov, and C. R. Simovski, Electromagnetics **17**, 213 (1997).
[30] R. Marques, F. Medina, and R. Rafii-El-Idrissi, Phys. Rev. B **65**, 144440 (2002).
[31] R. Marques, F. Mesa, J. Martel, and F. Medina, IEEE Trans. Antennas Propag. **51**, 2572 (2003).
[32] J. Garcia-Garcia, F. Martin, J. D. Baena, R. Marques, and L. Jelinek, J. Appl. Phys. **98**, 033103 (2005).
[33] K. Aydin, I. Bulu, K. Guven, M. Kafesaki, C. M. Soukoulis, and E. Ozbay, New J. Phys. **7**, 168 (2005).
[34] J. D. Jackson, *Classical Electrodynamics*, 3rd ed. (Wiley, New York, 1999).
[35] C. M. Butler, IEEE Trans. Antennas Propag. **AP-32**, 226 (1984).
[36] We note that some previous analytical calculations (say, Ref. 35) predicted that the current distribution along a thin metallic strip should be a *Maxwellian* form in which the current density diverges on the edges of the metallic strip. For the case that we studied, as the wavelength we considered is much larger than the width of the ring, the current in a Maxwellian form is almost uniform in the strip except in the region very close to the edges (see Ref. 35), which is indeed the case found in our FDTD simulations. However, since our FDTD mesh is not dense enough, we failed to find the divergences near the edges (see Fig. 1). Nevertheless, we note that the uniform distribution that we took is still a valid (although quite rough) approximation of the true current distribution and yields good results of resonance frequencies as compared with FDTD simulations (see Fig. 2). The reason of such good agreement is also partly due to the fact that the resonance frequency is a variational quantity which does not depend much on the detailed forms of the current distribution.